Supporting Information

Effect of an Amyloidogenic SARS-COV-2 Protein Fragment on α-synuclein Monomers and Fibrils

Asis K. Jana, Chance W. Lander, Andrew D. Chesney and Ulrich H. E. Hansmann**

Department of Chemistry & Biochemistry, University of Oklahoma, Norman, OK 73019, USA.

E-mail: jana.asis@gmail.com; uhansmann@ou.edu

Supporting information contains seven supporting figures (S1-S7).

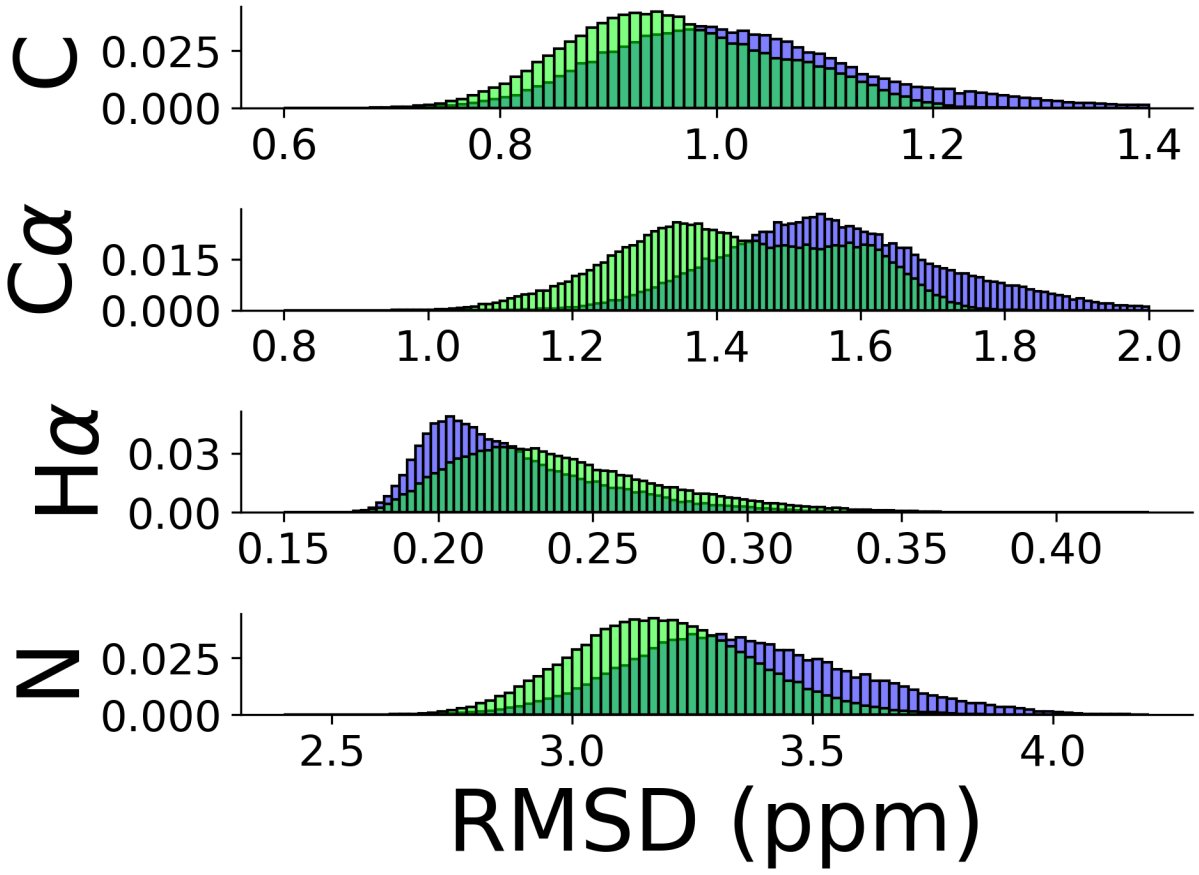

Figure S1: Root-mean-square-deviation (RMSD) between chemical shift data calculated in our monomer trajectories and the experimentally measured values. Data for the first μs are drawn in blue and such from the last two μs in green.

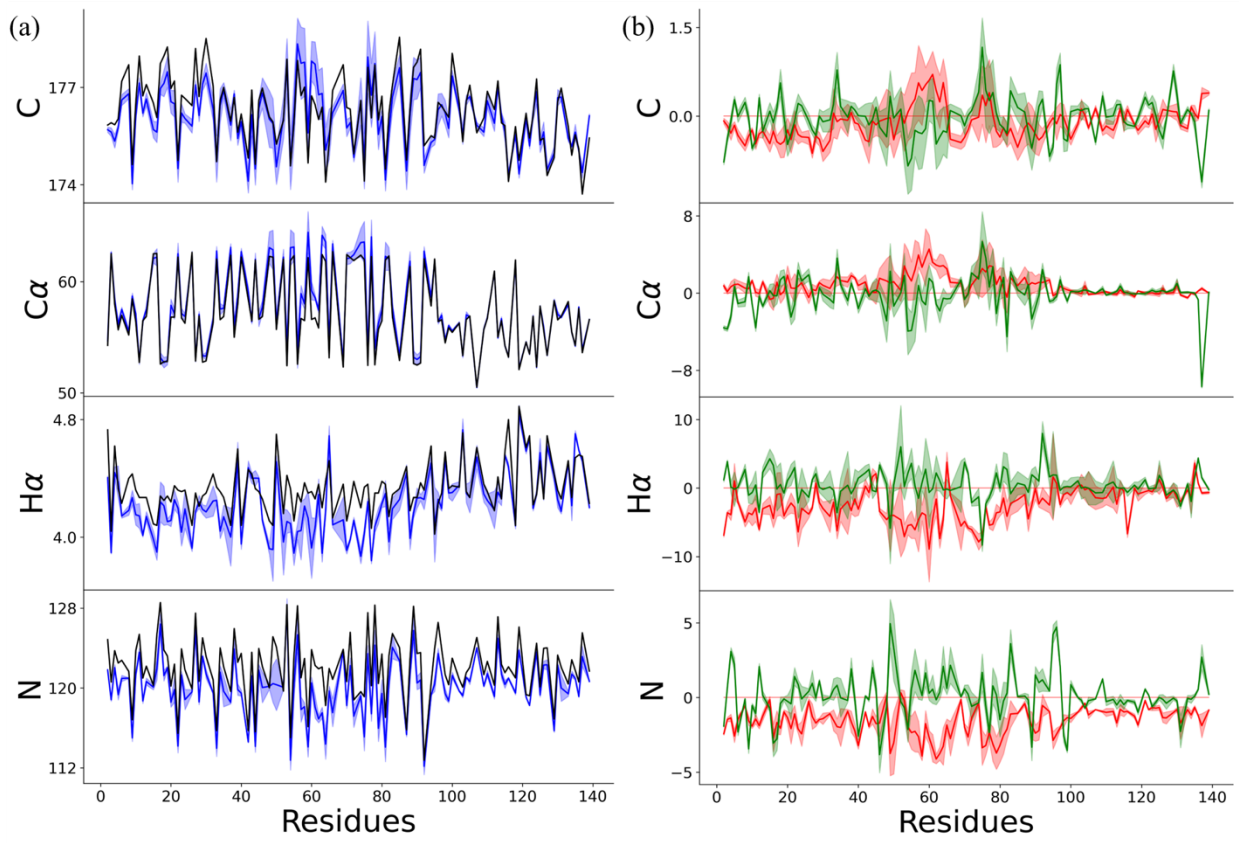

Figure S2: (a) Chemical shifts of carbonyl carbons (C), α-carbons (Cα), hydrogen atoms attached to α-carbons (Hα), and amide nitrogens (N) for α-synuclein monomer, as taken from NMR[1] (in black) and simulations (in blue). (b) Percentage change in chemical shift values with respect to experimentally measured values (red) and to that of random coil configurations (green) are shown in (b), with the black line marking zero deviation.

[1]*Rao, J. N.; Kim, Y. E.; Park, L. S.; Ulmer, T. S. Effect of Pseudorepeat Rearrangement on Alpha-Synuclein Misfolding, Vesicle Binding, and Micelle Binding. J. Mol. Biol.,* ***2009****, 390 (3), 516–529*

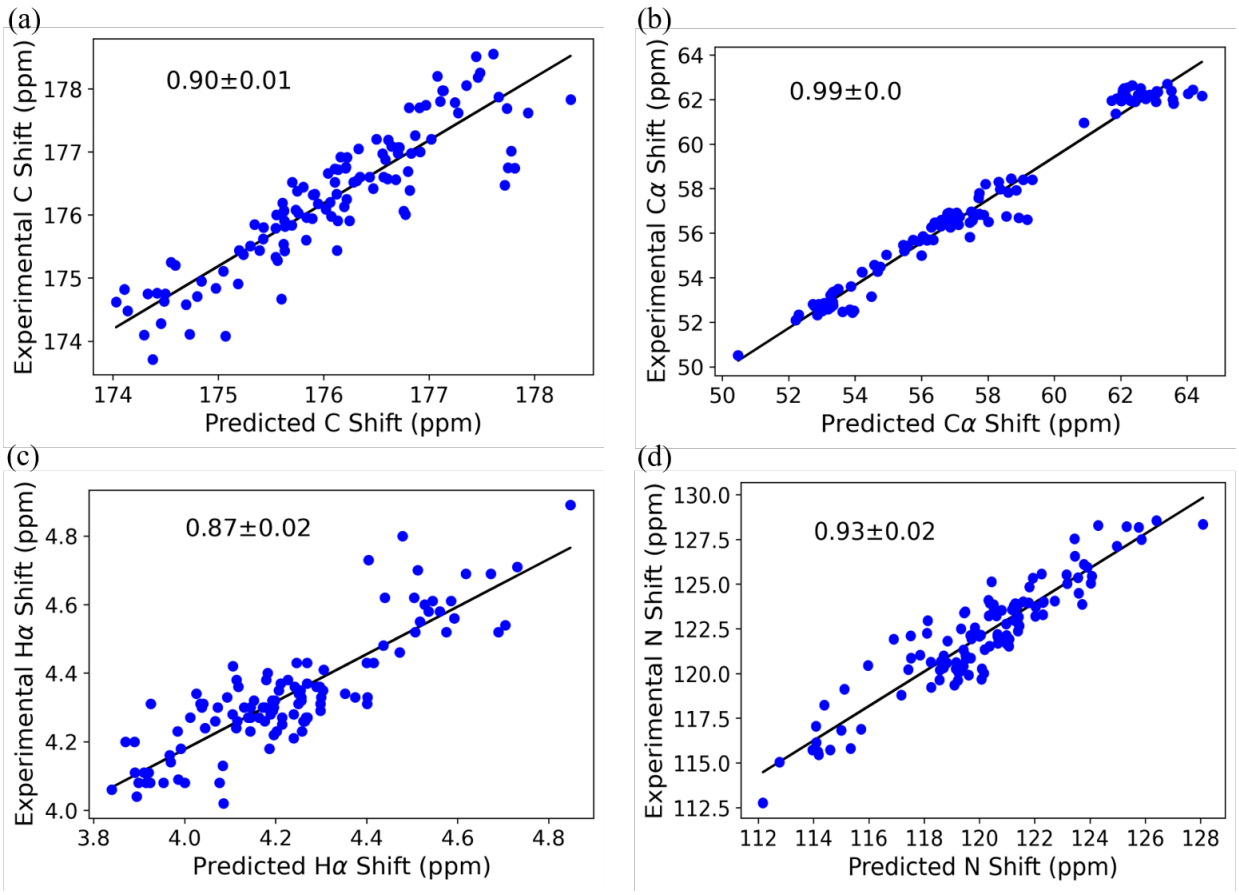

Figure S3: Regression plots of experimental (BMRB database entry 6968) over calculated C, Cα N and Hα chemical shifts for wild-type full-length α-synuclein monomer simulations are shown in (c). The Pearson correlation coefficients are also shown.

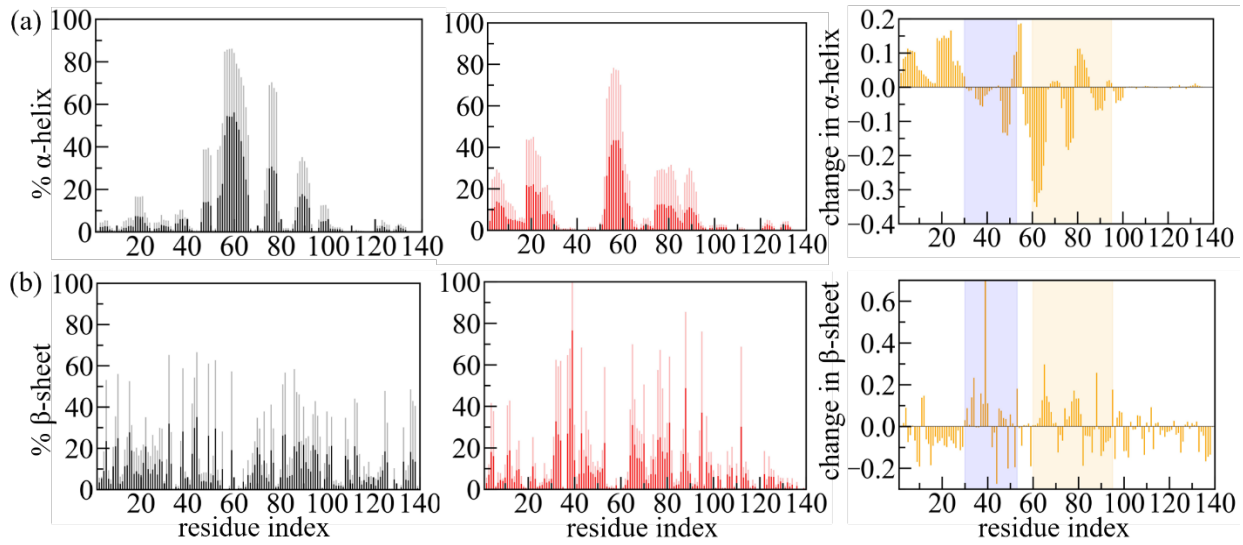

Figure S4: Residue-based α-helix (a) and β-sheet (b) propensity of wild-type α-synuclein monomer in absence (black, left panel)) and presence (red, central panel)) of the SK9- segment. The difference in the respective residue-wise propensities is drawn in the right panel (yellow). Familial mutation sites (A30-A53) and NAC regions (K60-V95) are highlighted in light blue and yellow, respectively.

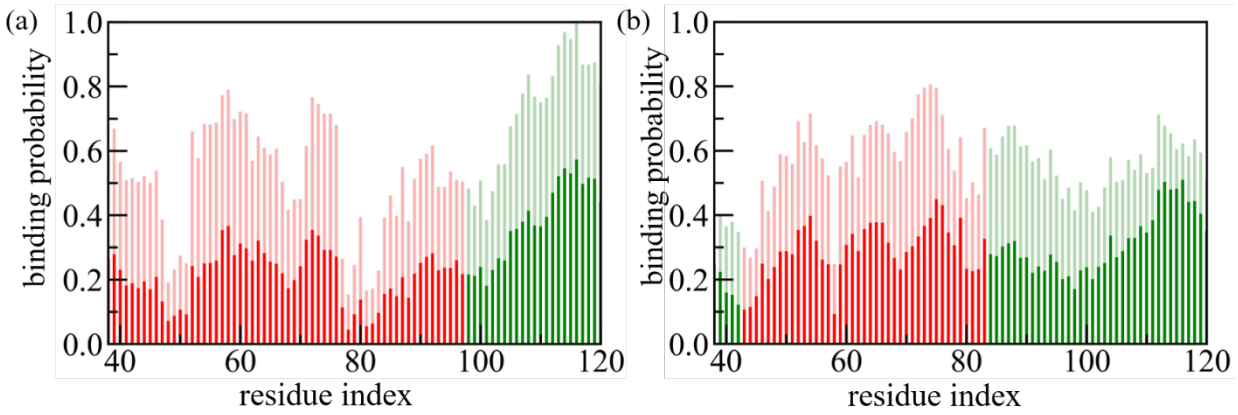

Figure S5: The residue-wise normalized binding probability of the SK9 segment for α-synuclein rod (a) and twister (b) polymorph, where the individual chains are extended to residues 38-120. Data are averaged over the final 50 ns of each trajectory and shaded region represents the standard deviation. Binding frequencies for the experimentally resolved segments are colored in red, while binding frequencies for the unresolved parts are drawn in green.

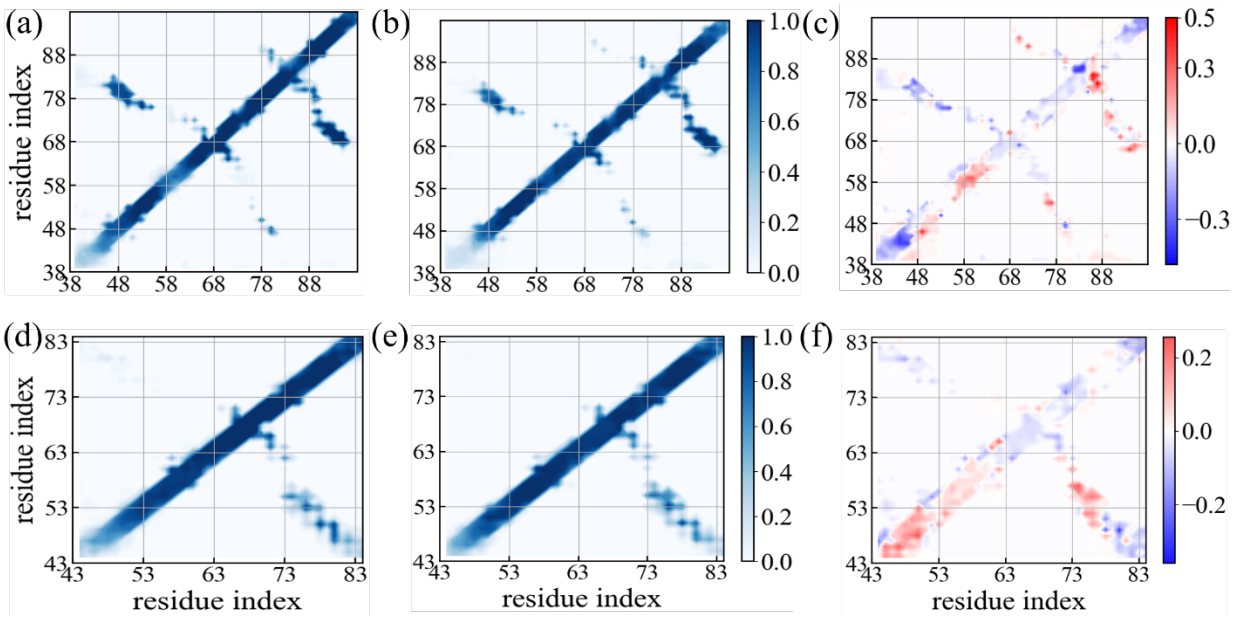

Figure S6: Residue-wise stacking contact probabilities measured in simulations of the rod-like fibril in absence (a) and presence of (b) SK9 segment. Corresponding data measured in simulations of the twister-like fibril are shown in (d) and (e). The differences in contact probability resulting from presence of SK9 are shown in (c) and (f), respectively. Data are from simulations where the individual chains are extended to residues 38-120. averaged over the final 50 ns of each trajectory, and calculated only for the experimentally resolved regions.

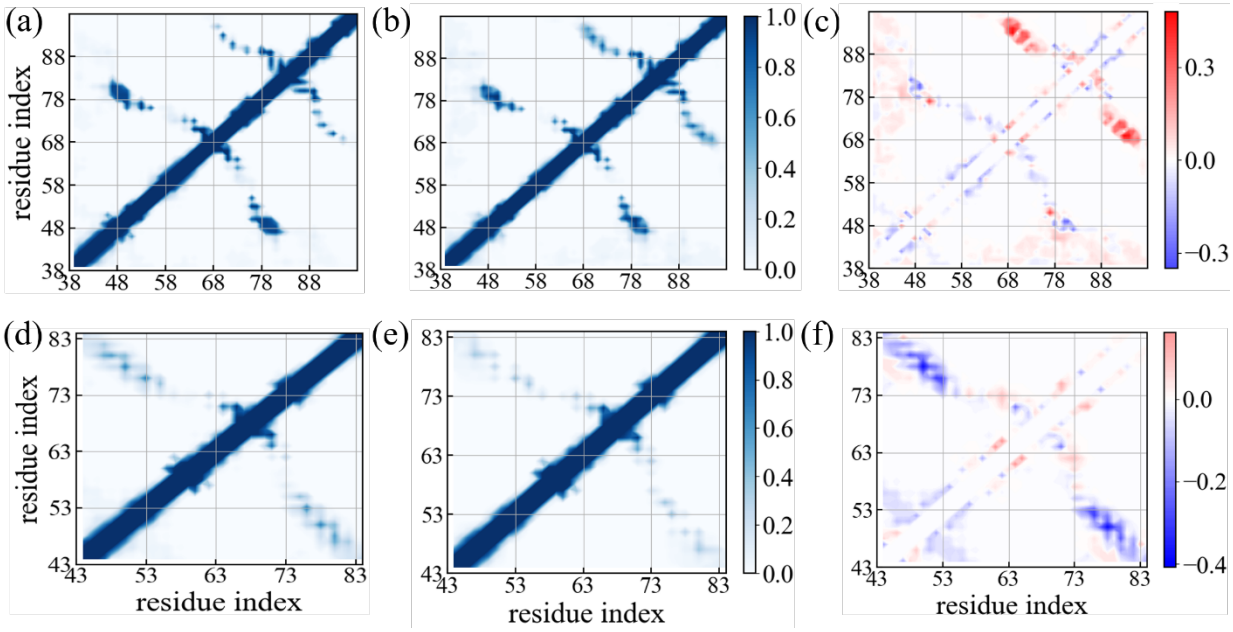

Figure S7: Residue-wise intrachain contact probabilities measured in simulations of the rod-like fibril in absence (a) and presence of (b) SK9 segment. Corresponding data measured in simulations of the twister-like fibril are shown in (d) and (e). The differences in contact probability resulting from presence of SK9 are shown in (c) and (f), respectively. Data are from simulations where the individual chains are extended to residues 38-120. averaged over the final 50 ns of each trajectory, and calculated only for the experimentally resolved regions.